Ligand-Directed Conformational Control over Porphyrinic Zirconium Metal−Organic Frameworks for Size-Selective Catalysis

Liting Yang,[#] Peiyu Cai,[#] Liangliang Zhang,[#] Xiaoyi Xu, Andrey A. Yakovenko, Qi Wang, Jiandong Pang, Shuai Yuan, Xiaodong Zou, Ning Huang,* Zhehao Huang,* and Hong-Cai Zhou*

ACCESS | Metrics & More | Article Recommendations | SI Supporting Information

ABSTRACT: Zirconium-based metal−organic frameworks (Zr-MOFs) have aroused enormous interest owing to their superior stability, flexible structures, and intriguing functions. Precise control over their crystalline structures, including topological structures, porosity, composition, and conformation, constitutes an important challenge to realize the tailor-made functionalization. In this work, we developed a new Zr-MOF (PCN-625) with a **csq** topological net, which is similar to that of the well-known PCN-222 and NU-1000. However, the significant difference lies in the conformation of porphyrin rings, which are vertical to the pore surfaces rather than in parallel. The resulting PCN-625 exhibits two types of one-dimensional channels with concrete diameters of 2.03 and 0.43 nm. Furthermore, the vertical porphyrins together with shrunken pore sizes could limit the accessibility of substrates to active centers in the framework. On the basis of the structural characteristics, PCN-625(Fe) can be utilized as an efficient heterogeneous catalyst for the size-selective [4 + 2] hetero-Diels−Alder cycloaddition reaction. Due to its high chemical stability, this catalyst can be repeatedly used over six times. This work demonstrates that Zr-MOFs can serve as tailor-made scaffolds with enhanced flexibility for target-oriented functions.
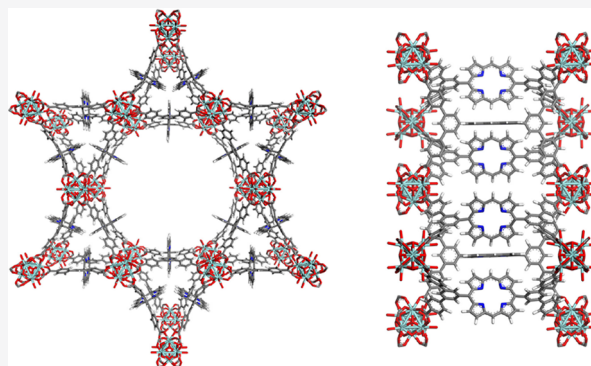
INTRODUCTION

Over the past decades, metal−organic frameworks (MOFs) have emerged as new types of crystalline materials, which allow the assembly of different organic ligands with metal ions or metal clusters by coordination bonds.[1−3] On the basis of reticular chemistry, both organic ligands and metal species can be considered as multitopic building blocks, which can be judiciously selected and integrated into MOFs to tune their properties for various purposes.[4] Due to their periodically ordered and atomically accurate structures, excellent porosity, flexible building blocks, and high tunability of properties, such as topologies, pore sizes, particle sizes, and acidity or alkalinity,[5] MOFs have been widely exploited for a large number of applications, including light emission,[6−8] gas adsorption,[9−11] gas separation,[12−14] heterogeneous catalysis,[15−26] drug delivery,[27−29] proton conduction,[30−33] and optoelectronics.[34−36]

Among the reported MOF materials, zirconium-based MOFs (Zr-MOFs) represent one class of specific examples with relatively high stability and structural flexibility. Particularly, the connectivity of the $[Zr_6O_4(OH)_8(COO)_8]$ (Zr_6) cluster can be well controlled through regulating the synthetic conditions. Up to now, five types of Zr_6 nodes with different connectivities have been reported, namely 12-, 10-, 8-, 6-, and 4-connected, leading to the generation of numerous Zr-

MOFs with different topologies, such as **csq**, **fcu**, **ftw**, **reo**, **scu**, and **spn**.[37,38] Consequently, many kinds of Zr-MOFs have been developed, including UiO-66,[39] PCN-222,[40] NU-1000,[41] PCN-223,[42] and PCN-224,[43] which possess various pore geometries and dimensions. The 8-connected PCN-222 and NU-1000 exhibit remarkable hydrothermal and chemical robustness in comparison with other MOFs. In the two MOFs, the Zr_6 nodes are connected with tetracarboxylate ligands, offering four coordination sites on each node as terminal and bridging hydroxyl units. Moreover, the large sizes of porphyrin- and pyrene-based tetracarboxylate ligands cause a long distance (>1.0 nm) to exist between adjacent Zr_6 clusters, permitting the insertion or grafting of small guest species into their porous skeletons. Consequently, three types of distinct pores are generated within the **csq**-net framework. The trigonal and hexagonal channels are formed along the *a* axis, while the rhombic channels are arrayed along the *c* axis.
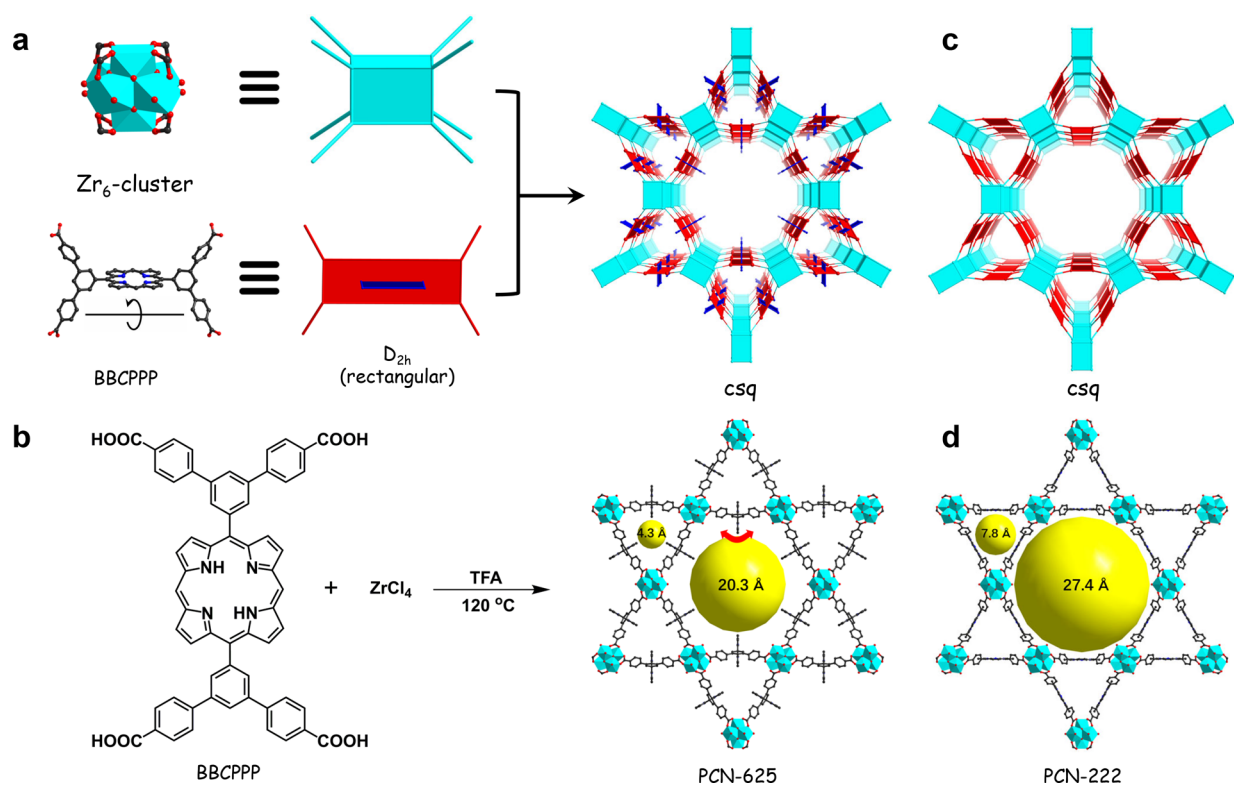
Figure 1. Schematic diagrams for the construction of PCN-625 and PCN-222. (a) Construction of PCN-625 using an 8-connected Zr_6 cluster and rectangular, 4-connected BBCPPP ligand. (b) Synthetic route for the construction of PCN-625 under solvothermal conditions. (c) The **csq** topology diagram of PCN-222. (d) Crystal structure of PCN-222 viewed along the c axis.

Recently, the Zr_6 node has been broadly utilized as a scaffold for the construction of MTV-MOFs on the basis of its tunable connectivity and remarkable stability.[44] As a robust and universal platform, Zr-MOFs enable the integration of metal ions, metal clusters, terminal ligands, and multicarboxylate linkers into the coordinatively unsaturated Zr_6 clusters. As a result, a series of more complex Zr-MOFs were developed on the basis of a postsynthetic retrosynthesis strategy, which exhibited plenty of opportunities to build potential architectures that have been impossible or difficult to implement. These special advantages give Zr-MOFs additional properties, further widening their application range.[45] Although many Zr-MOFs with the **csq** topology have been developed, all of them possess a similar pore environment, in which the cores of ligands are parallel to the channel walls. From the perspective of architectural design, it is of great interest to create different pore environments to accommodate specific guest species or satisfy new requirements. In this work, we developed a new type of porphyrin-based Zr-MOF with porphyrin rings vertical to the pore walls under the premise of maintaining the **csq** topology. Two kinds of isostructural MOFs with porphyrins were synthesized and unambiguously characterized. Due to the decreased pore sizes and increasing steric hindrance, the resulting PCN-625(Fe) exhibited highly size selective and efficient catalysis toward the [4 + 2] hetero-Diels–Alder cycloaddition of aldehydes with dienes. By a combination of the advantages of superior stability and high crystallinity, PCN-625(Fe) can be recycled over six times without significant loss of its activity.

■ EXPERIMENTAL SECTION

Materials. All of the chemicals were directly used after purchase from reagent companies. 3,5-Dibromobenzaldehyde, 4-carboethox-ybenzeneboronic acid, pyrrole, anhydrous indium(III) chloride, trifluoroacetic acid (TFA), dienes, and boron trifluoride diethyl etherate ($BF_3 \cdot Et_2O$) were purchased from Aldrich Chemical Co. Tetrakis(triphenylphosphine)palladium, potassium carbonate, and 2,3-dichloro-5,6-dicyano-1,4-benzoquinone (DDQ) were purchased from Ark Pharm, Inc. 1,4-Dioxane, zirconium chloride, and N,N-dimethylformamide (DMF) were purchased from Tokyo Chemical Industry Co., Ltd. (TCI). Iron(III) *meso*-tetraphenylporphine chloride (FeTPPCl) and aldehydes were purchased from Adamas. All of the air-sensitive operations were conducted under the protection of nitrogen on a standard Schlenk device.

Characterizations. Synchrotron powder X-ray diffraction was carried out on the 17-BM beamline at the Advanced Photon Source ($\lambda = 0.45236$ Å), Argonne National Laboratory, Argonne, IL, US. Powder X-ray diffraction (PXRD) measurements were performed on a Bruker D8-Advance X-ray diffraction system equipped with a Cu sealed tube ($\lambda = 1.54178$ Å). Proton nuclear magnetic resonance (^{1}H NMR) analysis was conducted on a Mercury 400 NMR spectrometer. Nitrogen sorption isotherms were collected on a Micromeritics ASAP 2020 instrument at 77 K. Thermogravimetric analysis (TGA) data were collected on a Shimadzu TGA-50 thermogravimetric analyzer at a heating rate of 10 °C min^{-1} under a nitrogen atmosphere. Elemental analysis was carried out on a vario EL cube Elementar. The surface morphologies of MOF samples were recorded with an FEI Quanta 600 scanning electron microscope (SEM). The conversion and yield values were determined on a Shimadzu QP2100 plus gas chromato-graph–mass spectrometer (GC-MS). Inductively coupled plasma-optical emission spectroscopic (ICP-OES) data were recorded using a Thermo iCAP6300 spectrometer.

Synthesis of Ligands. The synthesis routes and characterization results of bis[3,5-bis(4-carboxyphenyl)phenyl]porphyrin (BBCPPP)

and {bis[3,5-bis(4-carboxyphenyl)phenyl]porphyrinato} iron (Fe-BBCPPP) are described in the Supporting Information.

Synthesis of PCN-625. $ZrCl_4$ (20 mg, 0.086 mmol) and BBCPPP (10 mg, 0.011 mmol) were added to 2 mL of DMF. Then TFA (100 μL) was added to the solution as an acid modulator. The mixture was ultrasonically dissolved in a 5 mL high-pressure vessel, which was sealed and heated at 120 °C for 72 h. After the vial was slowly cooled to room temperature, purple crystallites were collected by filtration and rinsed with DMF and acetone. The obtained product was dried under vacuum, affording a yield of 77%.

Transmission Electron Microscopic (TEM) Analysis. The MOF samples for TEM characterization were dispersed in acetone. A droplet of the suspension was transferred onto a carbon-coated copper grid. The observation was carried out on a JEOL JEM2100 microscope, operated at 200 kV (Cs 1.0 mm, point resolution 0.23 nm). The images were recorded with a Gatan Orius 833 CCD camera (resolution 2048 × 2048 pixels, pixel size 7.4 μm) under low-dose conditions. Electron diffraction patterns were recorded with a Timepix QTPX-262k pixel detector (512 × 512 pixels, pixel size 55 μm, Amsterdam Sci. Ins.).

Continuous Rotation Electron Diffraction (cRED) Collection. The data were collected using the software Instamatic.[46−48] A single-tilt tomography holder was used for the data collection, which could tilt from −70° to +70° in the TEM. The aperture used for cRED data collection was about 1.0 μm in diameter. The speed of the goniometer tilt was 0.45° s^{-1}, and the exposure time was 0.5 s per frame. Data were collected within 4 min to minimize the beam damage and to maximize the data quality. The covered tilt angle was 103.6°.

Gas Sorption Measurement. Before the nitrogen sorption measurement, the freshly prepared PCN-625 (~100 mg) samples were first washed with DMF (10 mL × 3) and acetone (10 mL × 3), respectively. After that, the PCN-625 samples were soaked in anhydrous acetone (20 mL) for 24 h to completely exchange the nonvolatile DMF and remove residual metal ions or ligands. The samples were collected by centrifuging and activated by drying under vacuum at 100 °C prior to the nitrogen sorption analysis. Finally, the Zr-MOF samples were subjected to sorption measurement at 77 K.

Heterogeneous Catalysis. Activated PCN-625(Fe) (0.5 μmol) and $AgBF_4$ (1.0 μmol) were added to 2 mL of dry toluene in a 25 mL two-necked flask equipped with a Graham condenser. The mixture was stirred at room temperature for 5 h under a nitrogen atmosphere. After that, a toluene solution (4 mL) containing aldehydes (0.5 mmol) and diene (2.0 mmol) was added under a nitrogen atmosphere. The mixture was sealed and stirred at 80 °C. After filtration, the combined filtrate was concentrated by rotary evaporation and separated by column chromatography. The pure products were confirmed by NMR spectrometry.

Recycling of Catalyst. After each cycle, the PCN-625(Fe) catalyst was collected by filtration and thoroughly rinsed with tetrahydrofuran (10 mL × 3). Then PCN-625(Fe) was soaked in 20 mL of DMF overnight to remove any residual substrates or products trapped in the framework. Finally, PCN-625(Fe) was filtered, and washed with acetone (10 mL × 3), and dried under vacuum for 2 h for the use in the next cycle. All of the cycling experiments were performed under a nitrogen atmosphere in toluene with 2 mol % $AgBF_4$ as additive.

RESULTS AND DISCUSSION

Synthesis and Structural Characterization. In this work, we developed a new porphyrin-based Zr-MOF, denoted PCN-625, which was constructed with BBCPPP and Zr_6 clusters as building blocks under typical solvothermal conditions in the presence of TFA as a modulator (Figure 1a,b). The iron porphyrin ligand Fe-BBCPPP was also employed for the construction of PCN-625(Fe) under the same conditions. Similarly to other porphyrin-based Zr-MOFs, PCN-625 was obtained as deep purple crystals after a 72 h reaction. As shown in SEM images, the crystals of PCN-625

and PCN-625(Fe) exhibited a morphology of regular hexagonal prisms, which is in good accord with those of **csq**-net MOFs (Figure S1). These results indicated that PCN-625 exhibited a topological and crystalline structure similar to that of PCN-222 (Figure 1c,d). Elemental analyses of PCN-625 and PCN-625(Fe) agreed closely with theoretical values (Table S1). Due to the small crystal size of PCN-625, cRED collection was employed to resolve its crystal structure. Figure 2 shows the reconstructed 3D reciprocal lattice from the cRED
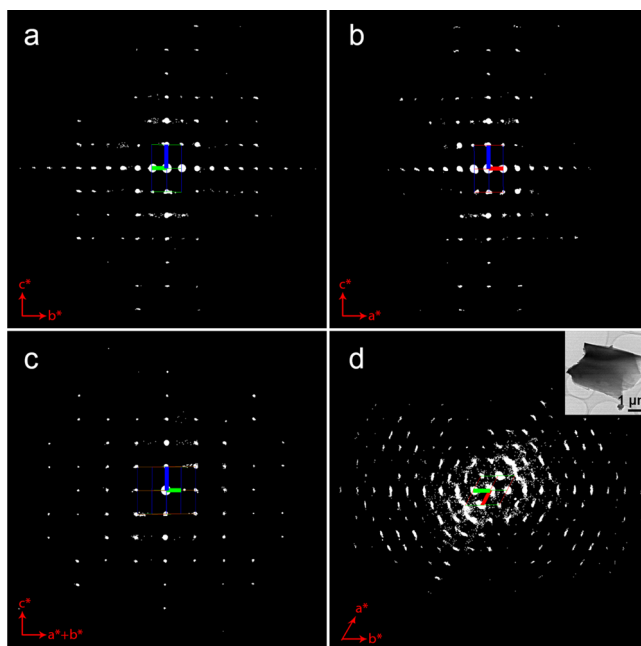

Figure 2. 2D slice cuts from the reconstructed 3D reciprocal lattice of PCN-625 showing the (a) 0kl, (b) h0l, and (c) hhl planes. (d) Projection of the reconstructed 3D reciprocal lattice along [001]. The inset shows the crystal from which the cRED data were collected.

data, revealing that PCN-625 has a primitive unit cell with parameters of a = 39.5 Å, b = 38.3 Å, c = 24.1 Å, α = 90.8°, β = 89.8°, and γ = 119.2°. As the lattice parameters a and b are very close and γ is around 120°, the possible crystal system could be hexagonal.

The two-dimensional (2D) slice cuts of the 3D reciprocal lattice at the 0kl (Figure 2a), h0l (Figure 2b), and hhl (Figure 2c) planes exhibited similar diffraction patterns, which confirms the hexagonal unit cell. No special reflection conditions can be deduced. Therefore, there are several possible space groups for PCN-625: $P6$ (No. 168), $P\bar{6}$ (No. 174), $P6/m$ (No. 175), $P6_22$ (No. 177), $P6mm$ (No. 183), $P\bar{6}2m$ (No. 189), $P\bar{6}m2$ (No. 187), and $P6/mmm$ (No. 191). The space group $P6/mmm$ with the highest symmetry was chosen for further structural determination on the basis of the projection of the reconstructed 3D reciprocal lattice along [001] (Figure 2d).

Due to the low crystallinity of the crystals, the resolution of the data set is low (~3.3 Å). A structure model was built according to the chemical and structural information (unit cell and space group). The optimization of the geometry was applied by using a pseudopotential plane-wave method within the DFT framework by the Accelrys Materials Studio package. After the creation of the initial structure, the geometry was quickly optimized in the FORCITE module with a Dreiding

c

force field. The structure model of PCN-625 was further refined against synchrotron powder X-ray diffraction (Figure 3). High-resolution PXRD data of PCN-625 was collected at
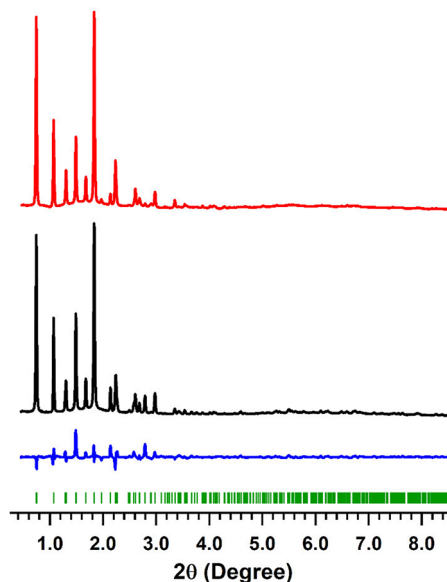

Figure 3. Rietveld refinement of PXRD patterns for PCN-625 (red curve, simulated; black curve, experimental; blue curve, difference profile; green bars, peak positions).

room temperature at 298 K (λ = 0.45236 Å). Rietveld refinement was performed using TOPAS Academic V5.1. The background of PCN-625 was fitted well with an 32nd-order Chebychev polynomial. The refinement was conducted using a Pearson VII type peak profile function, followed by the refinement of unit cells and zero shift. The Zr–O distances were soft-restrained to 2.20 Å. The guest species in the pores could not be located due to their partial occupancies and low symmetry. Instead, five oxygen atoms were added at random positions inside the pores to compensate for the contributions of the guest species, and refined subsequently. Finally, the R value was converged to R_p = 0.0592, R_{wp} = 0.0951, R_{exp} = 0.0730, and GOF = 1.302. The crystallographic details are shown in Table S2. PCN-625(Fe) exhibited almost the same PXRD patterns as those of PCN-625 (Figure S2), revealing they have the same crystal structures.

As shown in Figure 4a, each Zr$_6$ cluster links to eight BBCPPP ligands, while each BBCPPP ligand links to four Zr$_6$ clusters. Furthermore, the remaining terminal −OH groups on Zr centers supply the possibility to introduce additional functionalities. The resultant MOF exhibits a Kagome **csq** 3D net with two sets of 1D channels running along the c axis. One channel is mesoporous (20.3 Å), and the other is ultra-microporous (4.3 Å). Four porphyrins and two Zr$_6$ clusters form a nanocage (Figure 4b,c). The longer distance between adjacent porphyrin rings is about 10.8 Å, and the shorter distance is about 3.6 Å. PCN-625(Fe) displayed the same PXRD pattern as PCN-625, indicating both possess an identical crystalline structure except for the center metals.

Porosity and Chemical Stability. Moreover, PCN-625 exhibited high porosity and excellent chemical stability. The Brunauer−Emmett−Teller (BET) surface area of PCN-625 was determined to be 2658 m^2 g^{-1} (Figure S3), which is close to those of PCN-222 and NU-1000. In addition, the mesopore
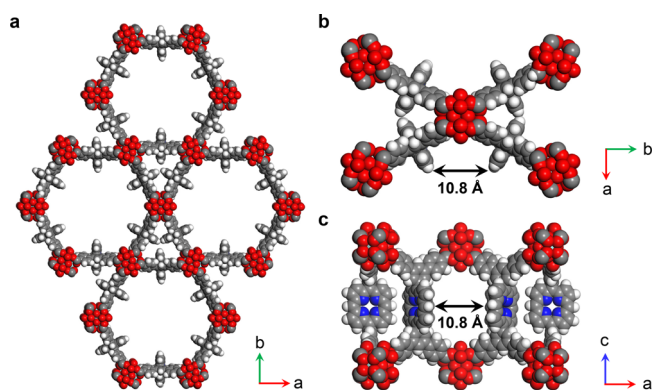

Figure 4. (a) Representative crystal structure of PCN-625 viewed along the c axis. (b) The crystal unit cell of PCN-625 viewed along the c axis. (c) The crystal unit cell of PCN-625 viewed along the b axis. The longer distance between adjacent porphyrin rings is about 10.8 Å.

size along the c axis was calculated as 2.1 nm (Figure S4), which is much smaller than those of PCN-222 and NU-1000 on account of the vertical porphyrin rings.[35,36] PCN-625(Fe) showed a BET surface area of up to 2600 m^2 g^{-1} (Figure S3) and the same mesopore size as that of PCN-625 (Figure S5). We further investigated the chemical stability of PCN-625 under different conditions, including water, boiling water, hexane, acetone, methanol, hydrochloric acid (6 M), concentrated hydrochloric acid, and sodium hydroxide (2 M) aqueous solutions. After soaked in these solvents for 72 h, the intensity of PCN-625 remained almost unchanged except in base solution (Figure S6). It was found that the PXRD pattern of base-soaked PCN-625 largely decreased, indicating decomposition under alkaline conditions. In addition, the residual mass percentage of PCN-625 was also evaluated (Figure S7). We found that the residual mass percentage of the soaked MOF samples in water, boiling water, hexane, and acetone was close to 100%. However, in methanol, hydrochloric acid (6 M), and concentrated hydrochloric acid, the values were determined to be 97%, 96%, and 95%, respectively. This result demonstrated that a small amount of PCN-625 decomposed after treatment in methanol, hydrochloric acid (6 M), and concentrated hydrochloric acid. The excellent framework stability of PCN-625 was also confirmed by N$_2$ sorption isotherms after the aforementioned treatment (Figure S8). All of the MOF samples maintained their original BET surface areas without significant loss. TGA measurement results indicated that PCN-625 is thermally stable up to 360 °C (Figure S9). Such high chemical stability is comparable with those of other Zr-MOFs.

Heterogeneous Catalysis in [4 + 2] Hetero-Diels−Alder Cycloaddition Reaction. By a combination of the advantages of high crystallinity, rich porosity, remarkable stability, and specific conformation, PCN-625(Fe) is considered to be an excellent candidate for selective heterogeneous catalysis. (1) The periodically ordered metalloporphyrin offers an ideal platform with atomically distributed catalytic sites, which is desirable for the development of high-performance catalysts. (2) The uniformly aligned mesoporous channels facilitate high-rate mass transfer, leading to an enhanced catalytic efficiency. (3) The exceptional chemical stability over a wide range of pH enables its feasibility and recyclability under substandard conditions. (4) The vertical porphyrin rings

could largely limit the access of substrates to catalytic metal centers, leading to a size- or shape-dependent catalysis.

We investigated the catalytic performance of PCN-625(Fe) for the [4 + 2] hetero-Diels−Alder cycloaddition using aldehydes and dienes as substrates.[49] This reaction is broadly utilized for the synthesis of pyrans, which constitute an important class of compounds involved in the field of fine chemicals and biological pharmaceuticals.[50] As was previously reported, the cationic Fe(III) porphyrins can efficiently activate electron-poor aldehydes, facilitating the chemoselective cycloaddition reaction with less reactive dienes. It was found that some kinds of weakly coordinating counteranions, such as SbF_6^- and BF_4^-, were necessary for high-performance catalysis.[51] The valence of iron in PCN-625(Fe) was determined as +3 according to the XPS profile (Figure S10), which exhibited two characteristic signals at 712.6 and 725.5 eV for Fe $2p_{3/2}$ or Fe $2p_{1/2}$ peaks, respectively. To accomplish this goal, an *in situ* anion metathesis using $AgSbF_6$ and $AgBF_4$ to displace the Cl^- with SbF_6^- and BF_4^- could be implemented in the catalysis process, generating the weakly coordinating PCN-625(Fe-SbF₆) and PCN-625(Fe-BF₄), respectively.

To screen the optimum catalytic conditions, we employed benzaldehyde (**1c**) and 2,3-dimethyl-1,3-butadiene (**2a**) as model compounds in the presence of PCN-625(Fe) as the catalyst (Table S3). Similarly to the reported homogeneous catalytic system,[46] the combination of toluene as the solvent, 1 mol % of PCN-625(Fe) as the catalyst, 2 mol % AgBF₄ as the additive, 80 °C, and 8 h afforded the best catalytic performance. With other solvents, including tetrahydrofuran, acetonitrile, and 1,4-dioxane, the yield was quite inferior (Table S3). Upon the screening of counteranions, the yield reached 99% with AgBF₄ as the additive. Other iron catalysts, such as $FeCl_3$, $FeCl_2$, FeF_3, $FeCl_3·2bpy$, and $FeCl_3·2tmeda$ species, as well as $AgSbF_6$ led to trace or lower yields. The reaction temperature, time, and amount of catalyst can make a difference in the catalytic performance (Table S3). To exclude other interference factors, we conducted three other control experiments with free-base PCN-625, a Zr₆ cluster, and NaBF₄ additive as catalysts for the selected model reaction. However, none of the species worked for the cycloaddition reaction. Moreover, the catalytic process would immediately terminate upon removal of PCN-625(Fe) by filtration, indicating that no homogeneous catalytic sites exist in the solution. To investigate the slight difference between conversion and yield, the used PCN-625(Fe) was hydrolyzed using a concentrated NaOH solution (6 M) after one catalytic cycle. A small percentage (2−3%) of products was detected in the digested solution, indicating that small portions of the products were probably trapped in the porous skeleton of PCN-625(Fe). In addition, approximately 1−2% of unknown byproducts were also detected in the reaction. Therefore, the difference between the conversion and yield can be attributed to the combined contribution of the porous texture of PCN-625(Fe) and side reactions. The enhanced catalytic performance can be attributed to the following two reasons: (1) the electron-withdrawing carbonate groups could decrease the electron density on active iron sites, which was confirmed by the DFT calculations (Table S4); (2) the Zr₆ cluster is also an electron-deficient unit, which could further reduce the peripheral electron density around the active sites and thus improve the activity.

Under the optimized conditions, we further expanded the substrate scope to other aldehydes and dienes with different dimensions (Tables S5 and S6). As shown in Table 1, when

Table 1. Catalytic Performance of PCN-625(Fe) in the [4 + 2] Hetero-Diels−Alder Cycloaddition Reaction Using Dienes and Aldehydes under Optimized Conditions[a]

[a]Reaction conditions: PCN-625(Fe) catalyst (1 mol %), aldehydes (0.5 mmol), and dienes (2.0 mmol) in 4.0 mL toluene at 80 °C.

aliphatic aldehydes with small dimensions were employed as substrates, such as acetaldehyde (**1a**; 6.2 × 3.6 Å²) and cyclopropanecarboxaldehyde (**1b**; 6.1 × 3.7 Å²), which can diffuse freely to approach the active sites, satisfactory yields were achieved (90% and 92% after 5 h, respectively). In contrast, the yield for the transformation of 2-naphthaldehyde (**1d**; 11.2 × 7.1 Å²) was calculated to be 56% after 5 h (Table S7). A complete conversion with a yield of 92% was realized after 24 h under the same conditions (Table S7). A yield of 86% was achieved using 1-naphthaldehyde (**1e**; 10.2 × 7.6 Å²) and **2a** as substrates. Notably, very low yields were observed for the bulky 4-phenoxybenzaldehyde (**1f**; 14.7 × 7.1 Å²) and 1-pyrenecarboxaldehyde (**1g**; 13.3 × 7.3 Å²) after 24 h. To evaluate the reactivity of these aldehydes, FeTPPCl was employed as a homogeneous catalyst under the same conditions. It was found that most of the aldehydes (**1a−f**) exhibited similar reactivities in the homogeneous system (Table S8). However, the reaction with **1g** afforded low conversion and yield values of 23% and 16%, respectively, which could be attributed to its low solubility in toluene. Therefore, the low conversion of **1f** suggested that the 10.8 Å nanopore was not wide enough to accommodate and then activate its bulky molecule, while the low conversion of **1g** could be ascribed to the combined contribution of its large molecule size and low solubility in the heterogeneous system. To investigate the electronic effects of substitutes on dienes, 2-methyl-1,3-butadiene (**2b**; 6.8 × 3.6 Å²) and 2-phenyl-1,3-

butadiene (2c; 11.5 × 7.4 Å^2) were employed to react with 1c, furnishing cycloadducts 3cb,cc in 94% and 83% yields, respectively. In comparison with 2a−c having less electron-donating methyl and phenyl groups, which seems to make no difference to the reactivity of dienes. Furthermore, 1-(1-methylene-2-propenyl)-4-phenylbenzene (2d; 15.2 × 10.6 Å^2) and 2,3-dibenzyl-1,3-butadiene (2e; 16.9 × 8.5 Å^2) were employed for the synthesis of 3cd,ce. However, no product was detected owing to their enormous molecule sizes.

The catalytic activities of PCN-625(Fe-BF$_4$), PCN-625, Fe-BBCPPP, AgBF$_4$, and AgSF$_6$ were evaluated using 1c and 2a as substrates under the optimized conditions (Table S9). PCN-625(Fe-BF$_4$) exhibited outstanding performance with a yield of 99%, which is the same as that of the in situ PCN-625(Fe) system. However, other catalysts, including PCN-625, Fe-BBCPPP, AgBF$_4$, and AgSF$_6$, were proved inactive, indicating each one cannot work alone for the cycloaddition reaction. Similarly to PCN-625(Fe), FeTPPCl can work effectively in the presence of AgBF$_4$ as an additive, suggesting that the unsaturated irons serve as active centers in the reaction.

To disclose the advantage of the specific conformation in PCN-625(Fe), control experiments with PCN-222(Fe)[40] and PCN-223(Fe)[42] as catalysts were conducted with 1a,f as aldehydes (Table S10), which have a large difference in size. PCN-222(Fe) exhibited almost the same catalytic performance toward 1a,f, while PCN-625(Fe) and PCN-223(Fe) showed much higher catalytic efficiency toward 1a than toward 1f. Moreover, additional control experiments with a mixture of 1a and 1f (molar ratio 1:1) were also conducted (Table S10). Interestingly, for the PCN-625(Fe) catalytic system, almost all of 1a was consumed while only a small portion (<2%) of 1f was involved. In contrast, PCN-222(Fe) only exhibited a medium efficiency for the transformation of 1a and 1f with conversion values of 58% and 53%, respectively. Thus, the size-selective advantage of PCN-625(Fe) can be attributed to the conformation change. Unlike PCN-222, which has active metal sites totally exposed to the 3.6 nm mesopores and can accommodate a broad range of substrates, PCN-625(Fe) exhibited an obvious catalytic selectivity.

The size-selective catalysis for [4 + 2] hetero-Diels−Alder cycloaddition was investigated using PCN-625(Fe), due to the specific conformation. To evaluate the catalytic performance of PCN-625(Fe), we compared its activity with those of other reported catalysts for the cycloaddition between 1c and 2a (Table S11). It was found that PCN-625(Fe) exhibited a performance superior to those of the reported UNLPF-16-Fe^{III},[52] FeP$_{p−H}$-HCP,[53] TrBF$_4$,[54] [Fe(TPP)]BF$_4$,[51,55] Sc-(OPf)$_3$,[56] and AlCl$_3$,[57] which required higher amounts of catalysts or longer reaction time but afforded lower yields. Meanwhile, due to their similar skeletal structures, its catalytic performance was almost the same as that of PCN-223(Fe).[42]

The reaction mechanism in this study was conjectured to be by five-coordinate and five-coordinate routes (Figure S11), which was proposed by Chung for the Fe-catalyzed hetero-Diels−Alder reaction. A concerted asynchronous process with the quartet and sextet states occurred in the two-mode reaction. In the five-coordinate mode, one of the coordinated aldehydes in an axial position dissociated with the formation of pentacoordinated iron species. The unsaturated iron would facilitate the chemospecific cycloaddition between diene and the inert C═O bond. However, the dienes could directly react with aldehydes in the saturated iron complex in the six-coordinate route. In addition, an oriented external electric field

and dispersion interactions can facilitate the reaction in MOF catalysis systems.

Recyclability. The robust skeleton of PCN-625(Fe) enables its repeated use in the cycloaddition reaction. We investigated its recyclability using the model reaction with 1c and 2a under similar conditions (Table S12). It was found that the PCN-625(Fe) catalyst can be recycled up to six times with only a modest loss of its reactivity (Figure S12). The catalyst can be simply separated by filtration and recovered by rinsing and soaking with some solvents, such as toluene, acetone, and tetrahydrofuran. The leaching amount of active iron species was further analyzed using ICP-OES measurements (Table S5). Although the amount of loss slowly increases along with the cycle number, only 3% of the iron was leached out after six cycles (Table S5). Interestingly, a significant loss can be detected after three runs. Furthermore, the influence of repeated utilization on the crystallinity and porosity of PCN-625(Fe) was evaluated. The PXRD measurement revealed that the catalyst could retain its high crystallinity over the whole six runs without a significant loss of intensity (Figure S13). However, its surface area gradually decreased after the third cycle, which is highly consistent with the leaching results (Figure S14).

CONCLUSION

In summary, we have rationally designed and synthesized a new type of porphyrin-based Zr-MOF material, in which the porphyrin ring adopted a vertical configuration to the pore surface. This specific configuration leads to the generation of shrunken cavities and channels, which can act as a nanoreactor for catalysis. In addition, this Zr-MOF exhibits high porosity and remarkable robustness under various conditions. In combination with the advantages of high crystallinity, rich porosity, distinct configuration, and excellent stability, PCN-625(Fe) displayed highly efficient size-selective catalysis toward the [4 + 2] hetero-Diels−Alder cycloaddition reaction with aldehydes and dienes as substrates. Importantly, the development of this particular Zr-MOF platform constitutes a further step forward tailor-made synthesis and functionalization.

ASSOCIATED CONTENT

Supporting Information

The Supporting Information is available free of charge at https://pubs.acs.org/doi/10.1021/jacs.1c03960.

Detailed synthesis procedures, characterization data for new compounds, and materials (PDF)

Accession Codes

CCDC 2087538 contains the supplementary crystallographic data for this paper. These data can be obtained free of charge via www.ccdc.cam.ac.uk/data_request/cif, or by emailing data_request@ccdc.cam.ac.uk, or by contacting The Cambridge Crystallographic Data Centre, 12 Union Road, Cambridge CB2 1EZ, UK; fax: +44 1223 336033.

AUTHOR INFORMATION

Corresponding Authors

Ning Huang − MOE Key Laboratory of Macromolecular Synthesis and Functionalization, State Key Laboratory of Silicon Materials, Department of Polymer Science and Engineering, Zhejiang University, Hangzhou 310027, People's Republic of China; Research Center for Intelligent

Sensing, Zhejiang Lab, Hangzhou 311100, People's Republic of China; ⓘ orcid.org/0000-0002-7021-8705;
Email: nhuang@zju.edu.cn

Zhehao Huang − *Berzelii Centre EXSELENT on Porous Materials, Department of Materials and Environmental Chemistry, Stockholm University, 10691 Stockholm, Sweden;*
ⓘ orcid.org/0000-0002-4575-7870;
Email: zhehao.huang@mmk.su.se

Hong-Cai Zhou − *Department of Chemistry, Texas A&M University, College Station, Texas 77843-3255, United States;* ⓘ orcid.org/0000-0002-9029-3788; Email: zhou@chem.tamu.edu

Authors

Liting Yang − *MOE Key Laboratory of Macromolecular Synthesis and Functionalization, State Key Laboratory of Silicon Materials, Department of Polymer Science and Engineering, Zhejiang University, Hangzhou 310027, People's Republic of China*

Peiyu Cai − *Department of Chemistry, Texas A&M University, College Station, Texas 77843-3255, United States*

Liangliang Zhang − *Department of Chemistry, Texas A&M University, College Station, Texas 77843-3255, United States;* ⓘ orcid.org/0000-0002-5091-018X

Xiaoyi Xu − *MOE Key Laboratory of Macromolecular Synthesis and Functionalization, State Key Laboratory of Silicon Materials, Department of Polymer Science and Engineering, Zhejiang University, Hangzhou 310027, People's Republic of China*

Andrey A. Yakovenko − *X-ray Science Division, Advanced Photon Source, Argonne National Laboratory, Argonne, Illinois 60439, United States*

Qi Wang − *Department of Chemistry, Texas A&M University, College Station, Texas 77843-3255, United States;* ⓘ orcid.org/0000-0002-8758-6168

Jiandong Pang − *Department of Chemistry, Texas A&M University, College Station, Texas 77843-3255, United States;* ⓘ orcid.org/0000-0001-7546-5580

Shuai Yuan − *Department of Chemistry, Texas A&M University, College Station, Texas 77843-3255, United States*

Xiaodong Zou − *Berzelii Centre EXSELENT on Porous Materials, Department of Materials and Environmental Chemistry, Stockholm University, 10691 Stockholm, Sweden;* ⓘ orcid.org/0000-0001-6748-6656

Complete contact information is available at:
https://pubs.acs.org/10.1021/jacs.1c03960

Author Contributions

[#]L.Y., P.C., and L.Z. contributed equally to this work.

Notes

The authors declare no competing financial interest.

■ REFERENCES

(1) Zhou, H.-C.; Long, J. R.; Yaghi, O. M. Introduction to Metal−Organic Frameworks. *Chem. Rev.* **2012**, *112*, 673−674.

(2) Schneemann, A.; Bon, V.; Schwedler, I.; Senkovska, I.; Kaskel, S.; Fischer, R. A. Flexible Metal−Organic Frameworks. *Chem. Soc. Rev.* **2014**, *43*, 6062−6096.

(3) Schoedel, A.; Li, M.; Li, D.; O'Keeffe, M.; Yaghi, O. M. Structures of Metal−Organic Frameworks with Rod Secondary Building Units. *Chem. Rev.* **2016**, *116*, 12466−12535.

(4) Yaghi, O. M. Reticular Chemistry−Construction, Properties, and Precision Reactions of Frameworks. *J. Am. Chem. Soc.* **2016**, *138*, 15507−15509.

(5) Howarth, A. J.; Liu, Y.; Li, P.; Li, Z.; Wang, T. C.; Hupp, J. T.; Farha, O. K. Chemical, Thermal and Mechanical Stabilities of Metal−Organic Frameworks. *Nat. Rev. Mater.* **2016**, *1*, 15018.

(6) Lustig, W. P.; Mukherjee, S.; Rudd, N. D.; Desai, A. V.; Li, J.; Ghosh, S. K. Metal−Organic Frameworks: Functional Luminescent and Photonic Materials for Sensing Applications. *Chem. Soc. Rev.* **2017**, *46*, 3242−3285.

(7) Yin, H.-Q.; Wang, X.-Y.; Yin, X.-B. Rotation Restricted Emission and Antenna Effect in Single Metal−Organic Frameworks. *J. Am. Chem. Soc.* **2019**, *141*, 15166−15173.

(8) Shustova, N. B.; McCarthy, B. D.; Dincă, M. Turn-On Fluorescence in Tetraphenylethylene-Based Metal−Organic Frameworks: An Alternative to Aggregation-Induced Emission. *J. Am. Chem. Soc.* **2011**, *133*, 20126−20129.

(9) Herm, Z. R.; Swisher, J. A.; Smit, B.; Krishna, R.; Long, J. R. Metal−Organic Frameworks as Adsorbents for Hydrogen Purification and Precombustion Carbon Dioxide Capture. *J. Am. Chem. Soc.* **2011**, *133*, 5664−5667.

(10) Sato, H.; Kosaka, W.; Matsuda, R.; Hori, A.; Hijikata, Y.; Belosludov, R. V.; Sakaki, S.; Takata, M.; Kitagawa, S. Self-Accelerating CO Sorption in a Soft Nanoporous Crystal. *Science* **2014**, *343*, 167−170.

(11) Krause, S.; Bon, V.; Senkovska, I.; Stoeck, U.; Wallacher, D.; Többens, D. M.; Zander, S.; Pillai, R. S.; Maurin, G.; Coudert, F.-X.; Kaskel, S. A Pressure-Amplifying Framework Material with Negative Gas Adsorption Transitions. *Nature* **2016**, *532*, 348−352.

(12) Lin, R.-B.; Xiang, S.; Xing, H.; Zhou, W.; Chen, B. Exploration of Porous Metal−Organic Frameworks for Gas Separation and Purification. *Coord. Chem. Rev.* **2019**, *378*, 87−103.

(13) Li, L.; Lin, R.-B.; Krishna, R.; Li, H.; Xiang, S.; Wu, H.; Li, J.; Zhou, W.; Chen, B. Ethane/Ethylene Separation in A Metal-Organic Framework with Iron-Peroxo Sites. *Science* **2018**, *362*, 443−446.

(14) Li, B.; Wang, H.; Chen, B. Microporous Metal−Organic Frameworks for Gas Separation. *Chem. - Asian J.* **2014**, *9*, 1474−1498.

(15) Zhu, L.; Liu, X.-Q.; Jiang, H.-L.; Sun, L.-B. Metal−Organic Frameworks for Heterogeneous Basic Catalysis. *Chem. Rev.* **2017**, *117*, 8129−8176.

(16) Feng, X.; Song, Y.; Li, Z.; Kaufmann, M.; Pi, Y.; Chen, J. S.; Xu, Z.; Li, Z.; Wang, C.; Lin, W. Metal−Organic Framework Stabilizes a Low-Coordinate Iridium Complex for Catalytic Methane Borylation. *J. Am. Chem. Soc.* **2019**, *141*, 11196−11203.

(17) Zeng, L.; Wang, Z.; Wang, Y.; Wang, J.; Guo, Y.; Hu, H.; He, X.; Wang, C.; Lin, W. Photoactivation of Cu Centers in Metal−Organic Frameworks for Selective CO_2 Conversion to Ethanol. *J. Am. Chem. Soc.* **2020**, *142*, 75−79.

(18) Jiao, L.; Zhang, R.; Wan, G.; Yang, W.; Wan, X.; Zhou, H.; Shui, J.; Yu, S.-H.; Jiang, H.-L. Nanocasting SiO_2 into Metal−Organic Frameworks Imparts Dual Protection to High-Loading Fe Single-Atom Electrocatalysts. *Nat. Commun.* **2020**, *11*, 2831.

(19) Huang, N.; Yuan, S.; Drake, H.; Yang, X.; Pang, J.; Qin, J.; Li, J.; Zhang, Y.; Wang, Q.; Jiang, D.; Zhou, H.-C. Systematic Engineering

of Single Substitution in Zirconium Metal−Organic Frameworks toward High-Performance Catalysis. *J. Am. Chem. Soc.* **2017**, *139*, 18590−18597.

(20) Pascanu, V.; Miera, G. G.; Inge, A. K.; Martín-Matute, B. Metal−Organic Frameworks as Catalysts for Organic Synthesis: A Critical Perspective. *J. Am. Chem. Soc.* **2019**, *141*, 7223−7234.

(21) Huang, N.; Wang, K.; Drake, H.; Cai, P.; Pang, J.; Li, J.; Che, S.; Huang, L.; Wang, Q.; Zhou, H.-C. Tailor-Made Pyrazolide-Based Metal−Organic Frameworks for Selective Catalysis. *J. Am. Chem. Soc.* **2018**, *140*, 6383−6390.

(22) Dhakshinamoorthy, A.; Asiri, A. M.; Garcia, H. Catalysis in Confined Spaces of Metal Organic Frameworks. *ChemCatChem* **2020**, *12*, 4732−4753.

(23) Dhakshinamoorthy, A.; Santiago-Portillo, A.; Asiri, A. M.; Garcia, H. Engineering UiO-66 Metal Organic Framework for Heterogeneous Catalysis. *ChemCatChem* **2019**, *11*, 899−923.

(24) Tanaka, K.; Nagase, S.; Anami, T.; Wierzbicki, M.; Urbanczyk-Lipkowska, Z. Enantioselective Diels−Alder Reaction in the Confined Space of Homochiral Metal−Organic Frameworks. *RSC Adv.* **2016**, *6*, 111436−111439.

(25) Chen, C.; Allen, C. A.; Cohen, S. M. Tandem Postsynthetic Modification of Metal−Organic Frameworks using An Inverse-Electron-Demand Diels−Alder Reaction. *Inorg. Chem.* **2011**, *50*, 10534−10536.

(26) Yadav, A.; Kanoo, P. Metal-Organic Frameworks as Platform for Lewis-Acid-Catalyzed Organic Transformations. *Chem. - Asian J.* **2019**, *14*, 3531−3551.

(27) Abanades Lazaro, I.; Forgan, R. S. Application of Zirconium MOFs in Drug Delivery and Biomedicine. *Coord. Chem. Rev.* **2019**, *380*, 230−259.

(28) Wu, M.-X.; Yang, Y.-W. Metal−Organic Framework (MOF)-Based Drug/Cargo Delivery and Cancer Therapy. *Adv. Mater.* **2017**, *29*, 1606134.

(29) Wang, X.-G.; Xu, L.; Li, M.-J.; Zhang, X.-Z. Construction of Flexible-on-Rigid Hybrid-Phase Metal-Organic Frameworks (MOFs) for Controllable Multi-Drug Delivery. *Angew. Chem., Int. Ed.* **2020**, *59*, 18078−18086.

(30) Ramaswamy, P.; Wong, N. E.; Shimizu, G. K. H. MOFs as Proton Conductors−Challenges and Opportunities. *Chem. Soc. Rev.* **2014**, *43*, 5913−5932.

(31) Wang, S.; Wahiduzzaman, M.; Davis, L.; Tissot, A.; Shepard, W.; Marrot, J.; Martineau-Corcos, C.; Hamdane, D.; Maurin, G.; Devautour-Vinot, S.; Serre, C. A Robust Zirconium Amino Acid Metal-Organic Framework for Proton Conduction. *Nat. Commun.* **2018**, *9*, 4937.

(32) Otake, K.; Otsubo, K.; Komatsu, T.; Dekura, S.; Taylor, J. M.; Ikeda, R.; Sugimoto, K.; Fujiwara, A.; Chou, C.-P.; Sakti, A. W.; Nishimura, Y.; Nakai, H.; Kitagawa, H. Confined Water-Mediated High Proton Conduction in Hydrophobic Channel of A Synthetic Nanotube. *Nat. Commun.* **2020**, *11*, 843.

(33) Nguyen, N. T. T.; Furukawa, H.; Gandara, F.; Trickett, C. A.; Jeong, H. M.; Cordova, K. E.; Yaghi, O. M. *J. Am. Chem. Soc.* **2015**, *137*, 15394−15397.

(34) Rice, A. M.; Martin, C. R.; Galitskiy, V. A.; Berseneva, A. A.; Leith, G. A.; Shustova, N. B. Photophysics Modulation in Photo-switchable Metal−Organic Frameworks. *Chem. Rev.* **2020**, *120*, 8790−8813.

(35) Zhou, Y.; Yu, F.; Su, J.; Kurmoo, M.; Zuo, J.-L. Tuning Electrical- and Photo-Conductivity by Cation Exchange within a Redox-Active Tetrathiafulvalene-Based Metal-Organic Framework. *Angew. Chem., Int. Ed.* **2020**, *59*, 18763−18767.

(36) Yang, L.; He, X.; Dinca, M. Triphenylene-Bridged Trinuclear Complexes of Cu: Models for Spin Interactions in Two-Dimensional Electrically Conductive Metal−Organic Frameworks. *J. Am. Chem. Soc.* **2019**, *141*, 10475−10480.

(37) Yuan, S.; Feng, L.; Wang, K.; Pang, J.; Bosch, M.; Lollar, C.; Sun, Y.; Qin, J.; Yang, X.; Zhang, P.; Wang, Q.; Zou, L.; Zhang, Y.; Zhang, L.; Fang, Y.; Li, J.; Zhou, H.-C. Stable Metal−Organic Frameworks: Design, Synthesis, and Applications. *Adv. Mater.* **2018**, *30*, 1704303.

(38) Chen, Z.; Hanna, S. L.; Redfern, L. R.; Alezi, D.; Islamoglu, T.; Farha, O. K. Reticular Chemistry in the Rational Synthesis of Functional Zirconium Cluster-Based MOFs. *Coord. Chem. Rev.* **2019**, *386*, 32−49.

(39) Øien, S.; Wragg, D.; Reinsch, H.; Svelle, S.; Bordiga, S.; Lamberti, C.; Lillerud, K. P. Detailed Structure Analysis of Atomic Positions and Defects in Zirconium Metal−Organic Frameworks. *Cryst. Growth Des.* **2014**, *14*, 5370−5372.

(40) Feng, D.; Gu, Z.-Y.; Li, J.-R.; Jiang, H.-L.; Wei, Z.; Zhou, H.-C. Zirconium-Metalloporphyrin PCN-222: Mesoporous Metal-Organic Frameworks with Ultrahigh Stability as Biomimetic Catalysts. *Angew. Chem., Int. Ed.* **2012**, *51*, 10307−10310.

(41) Deria, P.; Mondloch, J. E.; Tylianakis, E.; Ghosh, P.; Bury, W.; Snurr, R. Q.; Hupp, J. T.; Farha, O. K. Perfluoroalkane Functionalization of NU-1000 via Solvent-Assisted Ligand Incorporation: Synthesis and CO_2 Adsorption Studies. *J. Am. Chem. Soc.* **2013**, *135*, 16801−16804.

(42) Feng, D.; Gu, Z.-Y.; Chen, Y.-P.; Park, J.; Wei, Z.; Sun, Y.; Bosch, M.; Yuan, S.; Zhou, H.-C. A Highly Stable Porphyrinic Zirconium Metal−Organic Framework with shp-a Topology. *J. Am. Chem. Soc.* **2014**, *136*, 17714−17717.

(43) Feng, D.; Chung, W.-C.; Wei, Z.; Gu, Z.-Y.; Jiang, H.-L.; Chen, Y.-P.; Darensbourg, D. J.; Zhou, H.-C. Construction of Ultrastable Porphyrin Zr Metal−Organic Frameworks through Linker Elimination. *J. Am. Chem. Soc.* **2013**, *135*, 17105−17110.

(44) Yuan, S.; Qin, J.-S.; Li, J.; Huang, L.; Feng, L.; Fang, Y.; Lollar, C.; Pang, J.; Zhang, L.; Sun, D.; Alsalme, A.; Cagin, T.; Zhou, H.-C. Retrosynthesis of Multi-component Metal−Organic Frameworks. *Nat. Commun.* **2018**, *9*, 808.

(45) Bai, Y.; Dou, Y.; Xie, L.-H.; Rutledge, W.; Li, J.-R.; Zhou, H.-C. Zr-based Metal−Organic Frameworks: Design, Synthesis, Structure, and Spplications. *Chem. Soc. Rev.* **2016**, *45*, 2327−2367.

(46) Cichocka, M. O.; Ångström, J.; Wang, B.; Zou, X.; Smeets, S. High-Throughput Continuous Rotation Electron Diffraction Data Acquisition via Software Automation. *J. Appl. Crystallogr.* **2018**, *51*, 1652−1661.

(47) Yuan, S.; Qin, J.-S.; Xu, H.-Q.; Su, J.; Rossi, D.; Chen, Y.; Zhang, L.; Lollar, C.; Wang, Q.; Jiang, H.-L.; Son, D. H.; Xu, H.; Huang, Z.; Zou, X.; Zhou, H.-C. [Ti$_8$Zr$_2$O$_{12}$(COO)$_{16}$] Cluster: An Ideal Inorganic Building Unit for Photoactive Metal−Organic Frameworks. *ACS Cent. Sci.* **2018**, *4*, 105−111.

(48) Wang, B.; Rhauderwiek, T.; Inge, A. K.; Xu, H.; Yang, T.; Huang, Z.; Stock, N.; Zou, X. A Porous Cobalt Tetraphosphonate Metal-Organic Framework: Accurate Structure and Guest Molecule Location Determined by Continuous-Rotation Electron Diffraction. *Chem. - Eur. J.* **2018**, *24*, 17429−17433.

(49) Tietze, L. F.; Kettschau, G. Hetero Diels-Alder Reactions in Organic Chemistry. *Top. Curr. Chem.* **1997**, *189*, 1−120.

(50) Liu, P.; Jacobsen, E. N. Total Synthesis of (+)-Ambruticin. *J. Am. Chem. Soc.* **2001**, *123*, 10772−10773.

(51) Fujiwara, K.; Kurahashi, T.; Matsubara, S. Cationic Iron(III) Porphyrin-Catalyzed [4 + 2] Cycloaddition of Unactivated Aldehydes with Simple Dienes. *J. Am. Chem. Soc.* **2012**, *134*, 5512−5515.

(52) Johnson, J. A.; Petersen, B. M.; Kormos, A.; Echeverría, E.; Chen, Y.-S.; Zhang, J. A New Approach to Non-Coordinating Anions: Lewis Acid Enhancement of Porphyrin Metal Centers in a Zwitterionic Metal−Organic Framework. *J. Am. Chem. Soc.* **2016**, *138*, 10293−10298.

(53) Dou, Z.; Xu, L.; Zhi, Y.; Zhang, Y.; Xia, H.; Mu, Y.; Liu, X. Metalloporphyrin-Based Hypercrosslinked Polymers Catalyze Hetero-Diels-Alder Reactions of Unactivated Aldehydes with Simple Dienes: A Fascinating Strategy for the Construction of Heterogeneous Catalysts. *Chem. - Eur. J.* **2016**, *22*, 9919−9922.

(54) El Remaily, M. A. E. A. A. A.; Naidu, V. R.; Ni, S.; Franzén, J. Carbocation Catalysis: Oxa-Diels−Alder Reactions of Unactivated Aldehydes and Simple Dienes. *Eur. J. Org. Chem.* **2015**, *2015*, 6610−6614.

(55) Yang, Y.; Zhang, X.; Zhong, L.-P.; Lan, J.; Li, X.; Li, C.-C.; Chung, L. W. Unusual KIE and Dynamics Effects in the Fe-Catalyzed Hetero-Diels-Alder Reaction of Unactivated Aldehydes and Dienes. *Nat. Commun.* **2020**, *11*, 1850.

(56) Hanamoto, T.; Sugimoto, Y.; Jin, Y. Z.; Inanaga, J. Scandium(III) Perfluorooctanesulfonate [Sc(OPf)$_3$]: A Novel Catalyst for the Hetero Diels−Alder Reaction of Aldehydes with Non-Activated Dienes. *Bull. Chem. Soc. Jpn.* **1997**, *70*, 1421−1426.

(57) Jian, W.; Qian, B.; Bao, H.; Li, D. AlCl$_3$ Catalyzed Oxa-Diels-Alder Reaction of Aromatic Aldehydes with Simple Dienes. *Tetrahedron* **2017**, *73*, 4039−4044.